SUPPLEMENTARY INFORMATION FOR

EttA binds to ribosome exit site and regulates translation by restricting ribosome and tRNA dynamics

Bo Chen [1], Grégory Boël [1,2,6], Yaser Hashem [3,6], Wei Ning [4], Jingyi Fei [4,5], Chi Wang [1], Ruben L. Gonzalez Jr. [4], John F. Hunt [1,2], and Joachim Frank [1,3]

[1] Department of Biological Sciences, Columbia University, New York, NY 10027, USA;

[2] Northeast Structural Genomics Consortium, Columbia University, New York, NY 10027, USA;

[3] Howard Hughes Medical Institute, Department of Biochemistry and Molecular Biophysics, Columbia University, New York, NY 10032, USA;

[4] Department of Chemistry, Columbia University, New York, NY 10027, USA;

[5] Present address: Department of Physics, Center for the Physics of Living Cells, University of Illinois at Urbana-Champaign, Urbana, IL 61801, USA (J. Fei).

[6] G. Boël and Y. Hashem contributed equally to this work.

Correspondence should be addressed to J. Frank or R.L.G.
e-mail jf2192@columbia.edu (JF) and rlg2118@columbia.edu (RLG),
voice (212) 305-9510 (JF) and (212) 854-1096 (RLG),
fax (212) 305-9500 (JF) and (212) 932-1289 (RLG).

Key words: protein translation regulation, ABC-F protein family, ribosome, cryo-EM, single-molecule FRET, YjjK

This file includes:

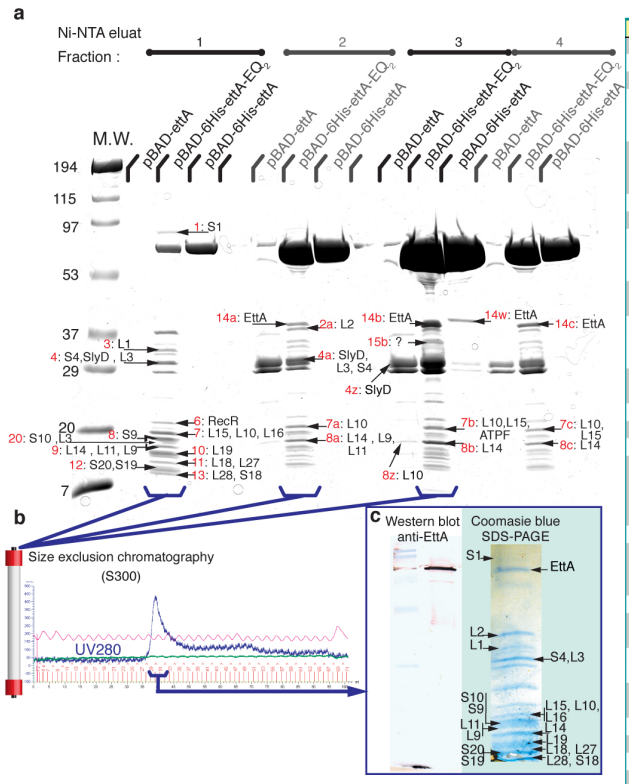

band	ID	pValue	Z-score	Score	Mw	Hits	Coverage
1	RS1_ECOLI	4.40E-06	3.14	0.56	61157	15	27%
2a	RL2_ECOLI	1.90E-09	4.17	0.26	29729	8	28%
3	RL1_ECOLI	1.00E-10	4.49	0.86	24598	9	33%
4	RS4_ECOLI	8.60E-11	4.51	1.61	23338	16	62%
	SLYD_ECOLI	2.50E-09	4.14	0.93	20853	6	31%
	RL3_ECOLI	3.20E-13	5.08	1.49	22243	10	46%
4a	SLYD_ECOLI	2.90E-13	5.09	0.7	20853	6	31%
	RL3_ECOLI	3.30E-10	4.37	0.65	22243	10	39%
	RS4_ECOLI	1.00E-10	4.5	0.7	23338	14	39%
4z	SLYD_ECOLI	4.70E-07	3.47	0.27	20853	4	28%
6	RECR_ECOLI	2.90E-10	4.38	0.39	21963	4	19%
7	RL15_ECOLI	4.80E-10	4.32	0.86	14980	8	31%
	RL10_ECOLI	3.30E-09	4.1	0.67	17580	8	42%
	RL16_ECOLI	4.70E-09	4.06	0.63	15281	9	40%
7a	RL10_ECOLI	3.30E-04	2.41	0.4	17580	10	54%
	RPOE_ECOLI	5.40E-05	2.74	0.37	21695	8	35%
7b	RL10_ECOLI	7.30E-08	3.72	0.69	17580	12	63%
	RL15_ECOLI	8.30E-07	3.39	0.54	14980	13	58%
	ATPF_ECOLI	3.90E-07	3.49	0.33	17264	4	21%
7c	RL10_ECOLI	3.90E-11	4.6	0.62	17580	10	59%
	RL15_ECOLI	9.00E-10	4.25	0.3	14980	9	38%
8b	RL14_ECOLI	1.50E-11	4.7	0.41	13541	7	34%
8c	RL14_ECOLI	6.40E-10	4.29	1.53	13541	10	38%
8	RS9_ECOLI	5.10E-06	3.12	0.57	14725	10	59%
8a	RL14_ECOLI	2.00E-13	5.13	1.86	13541	9	44%
	RL9_ECOLI	4.20E-11	4.59	0.38	15769	10	48%
	RL11_ECOLI	4.30E-10	4.34	0.28	14744	5	33%
	RL14_ECOLI	8.60E-11	4.51	0.28	13541	4	34%
8z	RL10_ECOLI	1.20E-06	3.33	0.18	17580	5	18%
9	RL14_ECOLI	2.80E-10	4.39	1.6	13541	9	55%
	RL11_ECOLI	4.90E-11	4.57	0.98	14744	7	43%
	RL9_ECOLI	7.90E-09	4	0.54	15769	10	54%
10	RL19_ECOLI	7.80E-10	4.27	0.65	13002	7	48%
11	RL18_ECOLI	1.10E-07	3.66	0.38	12769	8	43%
	RL27_ECOLI	4.50E-07	3.47	0.33	8993	8	63%
12	RS20_ECOLI	4.20E-06	3.15	0.47	9553	9	36%
	RS19_ECOLI	6.90E-06	3.07	0.28	10299	7	69%
13	RL28_ECOLI	1.60E-13	5.15	1.08	8875	6	58%
	RS18_ECOLI	2.20E-10	4.41	0.43	8855	3	26%
14b	YJJK_ECOLI	6.40E-13	5.02	1.05	62311	13	34%
14c	YJJK_ECOLI	3.60E-10	4.36	1.79	62311	22	41%
14w	YJJK_ECOLI	5.60E-15	5.46	0.85	62311	15	30%
20	RS10_ECOLI	3.00E-06	3.2	0.44	11735	7	41%
	RL3_ECOLI	7.10E-08	3.72	0.31	22243	9	20%

Supplementary Figure 1. ***In vivo*** **pull-down of His$_6$-EttA-EQ$_2$ with 70S ribosome.** Strain MG1655-*ettA::Tn5* carrying either the plasmids, pBAD-*ettA*, pBAD-His$_6$-*ettA* or pBAD-His$_6$-*ettA*-EQ$_2$[1], were grown and protein over-expression was induced. After cells collection and lysis, an equal amount of total protein for each sample was loaded on three columns of Ni-NTA. The columns were washed and EttA was eluted into fractions. **(a)** Coomassie colored gel of the fractions for the different samples. From this gel some of the bands that specifically appeared in the pBAD-His$_6$-*ettA*-EQ$_2$ sample compared to the pBAD-His$_6$-*ettA* (if an equivalent was present in the control pBAD-*ettA* the band was also selected) were identified by peptide mass fingerprinting identification. These bands are labeled with red numbers. The identification of the protein(s) present in those bands is shown on the table (right side). The table shows the protein ID (Uniprot ID), the pValue, Z-score and Score calculated by Aldente, the predicted molecular weight (Mw), the number of peptides detected for each identification (Hits), the percentage of coverage of the peptides identified against the full protein (Coverage). **(b)** 5 liters culture of the strain MG1655-*ettA::Tn5* carrying pBAD-His$_6$-*ettA*-EQ$_2$ had been processed like the one presented in **(a)**. The fractions 1 to 5 after Ni-NTA pull-down were pooled, concentrated and run on a gel filtration column. A fast running peak with a high absorbance at 280 nm was detected in the void volume of the column, which corresponded to a molecular weight higher than 1.5 MDa. The fractions of this peak were pooled and concentrated. **(c)** This sample was separated on an SDS-PAGE gel that shows a full ribosome proteins profile. The sample also had been submitted to western-blot analysis with an affinity purified anti-EttA antibody to confirm the presence of EttA on this purified complex.

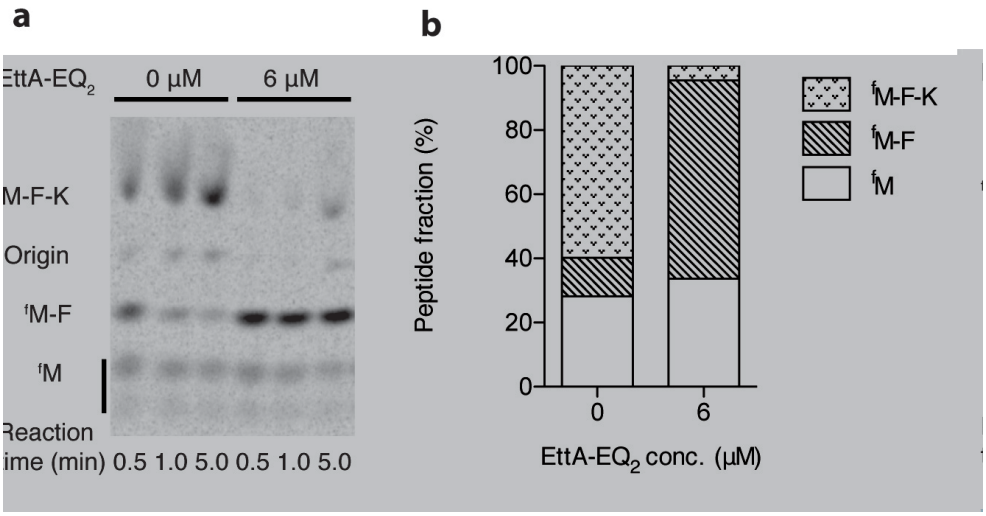

Supplementary Figure 2. Peptide formation assay in parallel with cryo-EM sample preparation. **(a)** 70S–mRNA–[^{35}S]fMet-tRNA^{fMet} initiation complex (0.5 μM), prepared in parallel with the 70S initiation complex used in cryo-EM study, was first mixed with EttA-EQ$_2$ (6 μM) or polymix buffer and incubated at 37 ºC for 1 min, then mixed with Phe-tRNA^{Phe}–EF-Tu–GTP and Lys-tRNA^{Lys}–EF-Tu–GTP ternary complexes (0.67 μM each) and incubated at 37 ºC for 1 min, then with EF-G (1.5 μM) and incubated at 37 ºC for indicated reaction time (Supplementary Methods). **(b)** Relative fractions of mono- (^{f}M), di- (^{f}M-F), and tri- (^{f}M-F-K) peptides in **(a)** after 1 min incubation with EF-G.

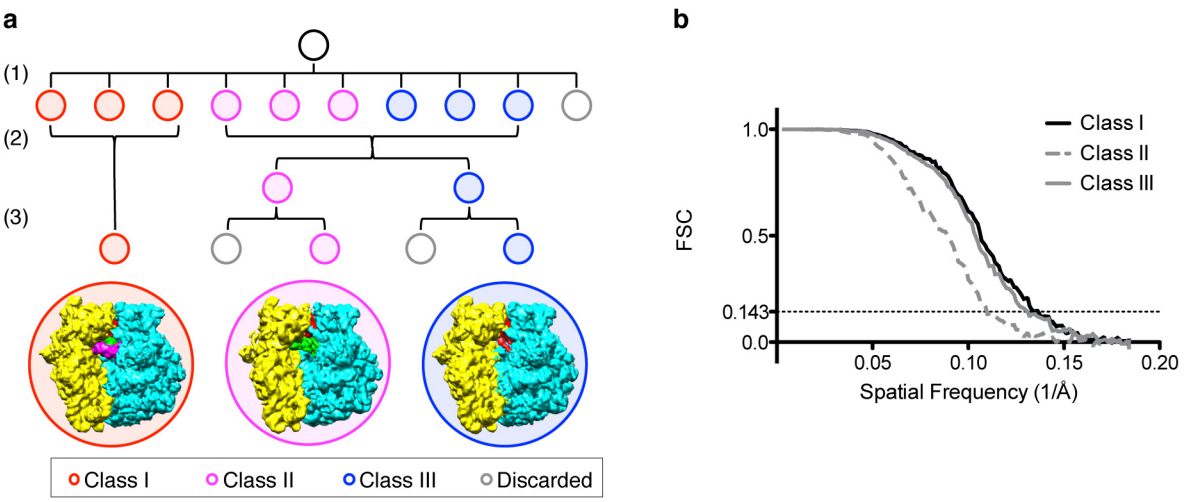

Supplementary Figure 3. Flow chart of RELION-based hierarchical classification and Fourier Shell Correlation (FSC) curves for reconstructions from the three classes. (a) RELION-based classification diagram. See computational classification of **Supplementary Note** for details. **(b)** FSC curve to determine the resolution of the reconstructions from the three classes. For each class, the two half-volumes were generated using RELION. The FSC between the two half-volumes was calculated using SPIDER (**Online Methods**). The resolution of each map was determined using FSC = 0.143 cutoff, yielding 7.5 Å (70S–EttA–$tRNA_2$, class I), 9.1 Å (70S–EttA–tRNA, class II) and 7.7 Å (70S–EttA, class III), respectively.

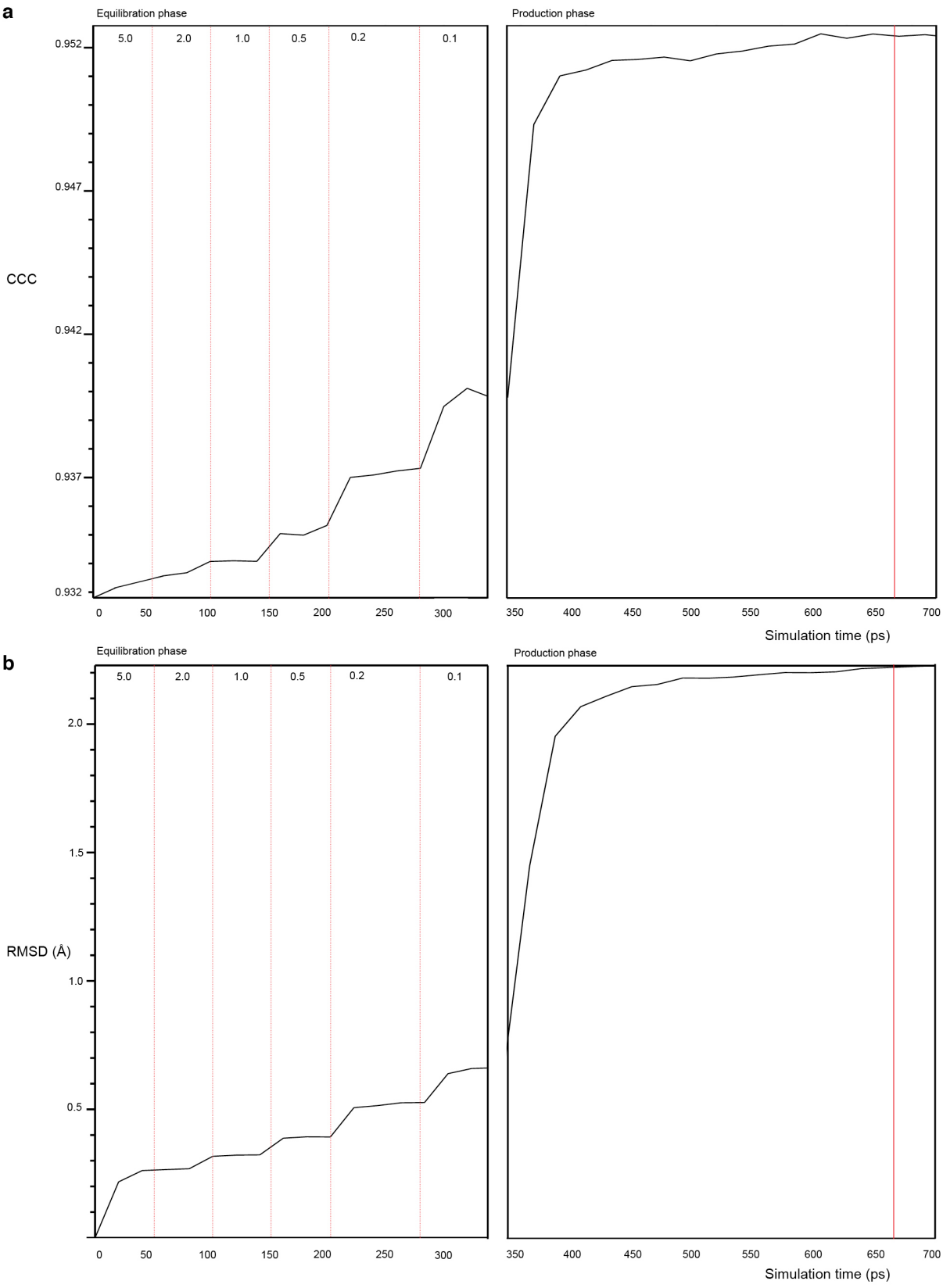
a
Equilibration phase
Production phase
5.0
2.0
1.0
0.5
0.2
0.1
CCC
0.952
0.947
0.942
0.937
0.932
0
50
100
150
200
250
300
350
400
450
500
550
600
650
700
Simulation time (ps)
b
Equilibration phase
Production phase
5.0
2.0
1.0
0.5
0.2
0.1
RMSD (Å)
2.0
1.5
1.0
0.5
0
50
100
150
200
250
300
350
400
450
500
550
600
650
700
Simulation time (ps)

Supplementary Figure 4. Root Mean Square Deviation (RMSD) and Cross-Correlation Coefficient (CCC) plots of the MDFF process. (a) CCC plotted *versus* the simulation time in picoseconds (ps). **(b)** RMSD plotted *versus* the simulation time in picoseconds. In both **(a)** and **(b)**, the MDFF equilibration phase (left plot) is distinct from the production phase (right plot). Dotted red lines separate consecutive stages of the equilibration phase conducted at decreasing positional harmonic constraints (in kcal/(mol×Å) at the top of the plots). The solid red line denotes the frame at which the convergence is considered achieved as it marks the beginning of a plateau.

Nature Structural and Molecular Biology: doi:10.1038/nsmb.2741

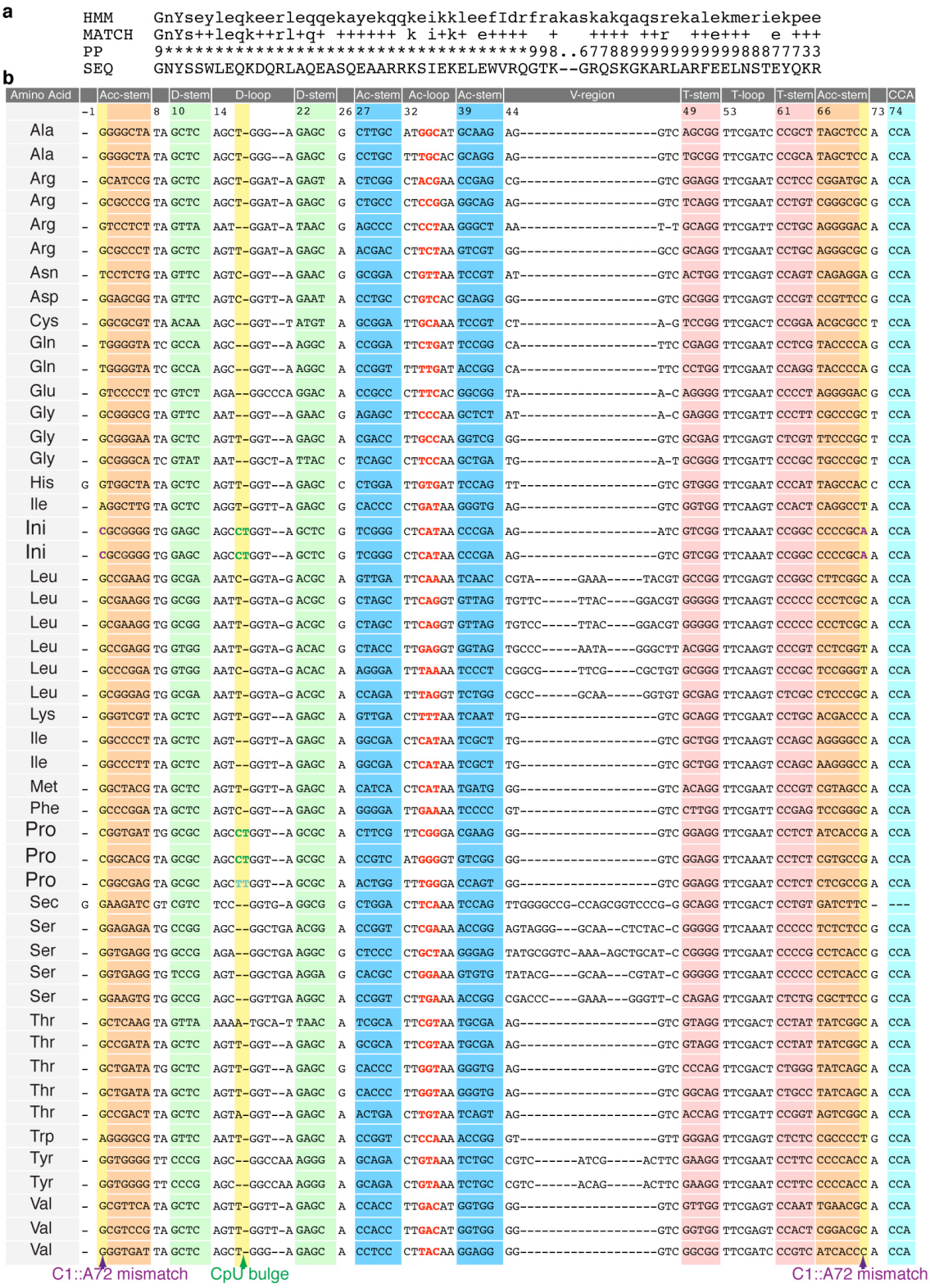

Supplementary Figure 5. Significant Pfam-A matches of PtIM of EttA with PF12848 (ABC_tran_2) domain[2], and Sequence alignment of *E. coli* K12-MG1655 tRNA coding genes. **(a)** HMM, hidden Markov model sequence; MATCH, the match between HMM and SEQ; PP, posterior probability, or the degree of confidence in each individual aligned residue; SEQ, query sequence. Green and cyan highlights residues in PtIM of EttA that may interact with

P-site $tRNA^{fMet}$ and with 23S rRNA, respectively (**Supplementary Table 1**). **(b)** An alignment of all the genes coding for tRNA in *E. coli* MG1655 was generated using the tRNAdb[3] database (http://trna.bioinf.uni-leipzig.de), highlighting the specific features of the initiator tRNA which may interact with ribosome-bound EttA-EQ_2. tRNA structural features that are close to EttA-EQ_2 are highlighted in yellow. The CpU bulge, present in two isoforms of Initiator tRNA (Ini) and two of three isoforms of Proline tRNA (Pro), is in green. The C1::A72 mismatch, only present in the two isoforms of initiator tRNA, is in purple. The anticodons of all the tRNAs are in red.

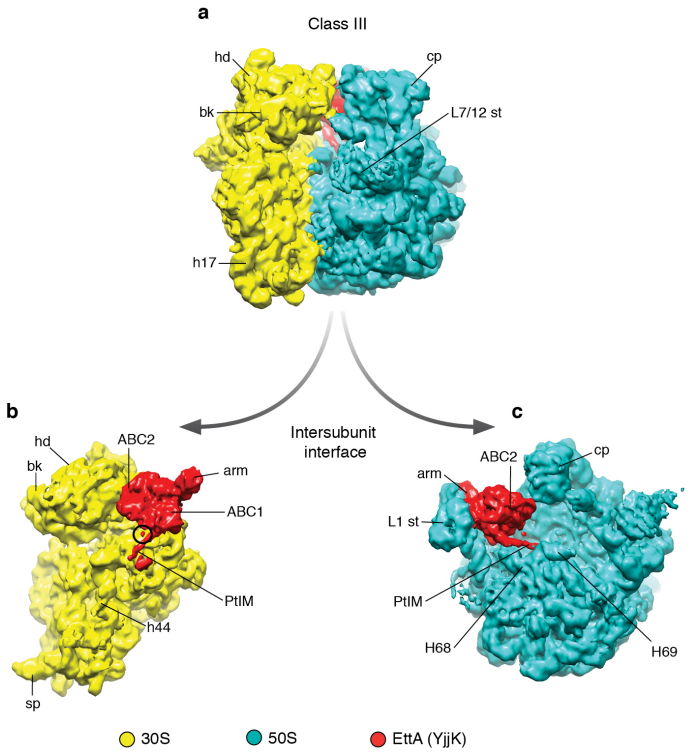

Supplementary Figure 6. cryo-EM 3D reconstruction of the class III 70S–EttA complex. Color scheme and abbreviations of landmarks are the same as **Fig. 1**. Circled region indicates the poorly defined distal end of the EttA PtIM.

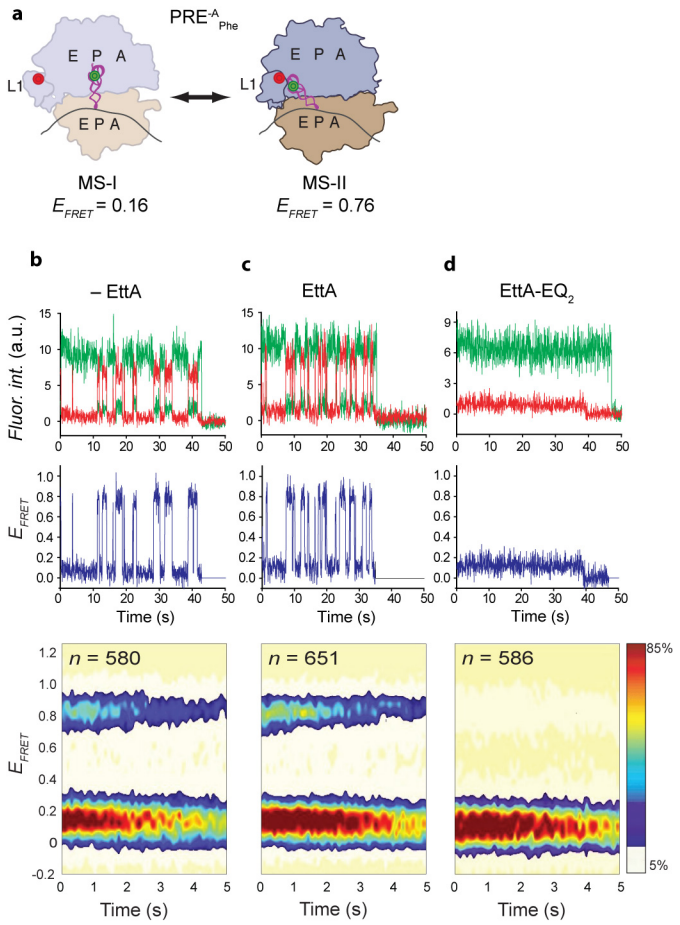

Supplementary Figure 7. EttA-mediated regulation of MS-I↔MS-II equilibrium as observed using smFRET$_{L1\text{-}tRNA}$ studies of a PRE$^{-A}_{Phe}$ complex. (a) Cartoon diagram of the conformational equilibrium of the PRE$^{-A}_{Phe}$ complex between the MS-I conformation harboring an open L1 stalk (ribosomal complex on left) and the MS-II conformation harboring a closed L1 stalk (ribosomal complex on right). The 30S subunit is shown as a tan cartoon, 50S subunit as a blue cartoon; tRNA^{Phe} as an orange ribbon; mRNA as a black curve; Cy3 FRET donor fluorophore as a green circle; and Cy5 FRET acceptor fluorophore as a red circle. **(b-d)** smFRET$_{L1\text{-}tRNA}$ experiments were recorded in the presence of 0.8 mM ATP and in **(b)** the absence of EttA, **(c)** the presence of 1.8 μM EttA, and **(d)** the presence of 1.8 μM EttA-EQ$_2$. 1st row: Representative Cy3 and Cy5 fluorescence intensity (*Flour. Int.*) *vs.* time trajectories. The fluorescence intensities are plotted in arbitrary units (a.u.) with the Cy3 fluorescence intensity plotted in green and the Cy5 fluorescence intensity plotted in red. 2nd row: The corresponding E_{FRET} *vs.* time trajectories. The E_{FRET} at each time point was calculated using $E_{FRET} = I_{Cy5} / (I_{Cy3} + I_{Cy5})$, where I_{Cy3} and I_{Cy5} are emission intensities of Cy3 and Cy5, respectively, and is plotted in blue. 3rd row: Surface contour plots of the time evolution of the population FRET. The contour plots were generated by superimposing individual E_{FRET} *vs.* time trajectories and the contours are colored from white (lowest-populated) to red (highest-populated). *N* denotes the number of E_{FRET} *vs.* time trajectories that were used to construct each contour plot.

SUPPLEMENTARY TABLES

Supplementary Table 1. Molecular contact regions between EttA and the 70S ribosome complex including P-site tRNA.

Contact Type [a]	EttA		Ribosome or tRNA		
	EttA domain	Approximate Position [c]	Ribosome subunit/ tRNA	Ribosomal /tRNA component [b]	Approximate Position [c]
p-r	**ABC β 1**	H9-R10, S26-S28, E62-Q66	**50S**	**23S H68**	G1857-G1860, U1883-A1885
p-p		P16-P17, K57-I59		**L33**	K26- K32
p-p	**Arm**	L104-A112	**50S**	**L1**	P118-R122, V145-N148
p-p		F118-A134			R53-G61, K141-N148
p-p		D136-V142			L127-V130
p-r		L139-V142		**23S H77**	G2168-A2170
p-r	**ABC α 1**	Q143-A150	**50S**	**23S H77**	G2112-A2114
p-r	**Core1**	I238-W240	**50S**	**23S H68**	A1848-U1851
p-r	**PtIM**	W247-K271	**50S**	**23S H68**	G1839-U1841, C1893-C1895
p-r		K267-K271		**23S H69**	C1925-A1927
p-r		W275-R283		**23S H93**	C2594-U2596
p-r		K281-K288		**23S H74**	U2075-A2077, A2434-G2437
p-t		E274-K281	**P-site tRNA^{fMet}**	**Acceptor stem**	G2-C3, G70-A72
p-t		N295-R305		**D-stem loop**	C17-U17a
p-r		R318-K322	**30S**	**16S h41-h42**	G1297-U1301, G1334-G1337
p-r	**ABC β 2**	T381-T385	**30S**	**16S h41-h42**	G1297-U1301
p-p		K322-E325		**S7**	K109-K113
p-p	**Toe**	G411-I414	**50S**	**L5**	A42-L48, R79-Y82
p-t	**ABC α 2**	K434-V436	**P-site tRNA^{fMet}**	**D-stem loop**	U17a-G18
p-t		R425-R430			G19-U20, C56
p-p		R441-E444	**50S**	**L33**	T28-P30
p-p	**Core2**	E521-N526	**30S**	**S7**	K109-G111, E122-K130
p-p	**C-terl Tail**	T528-Y533	**30S**	**S7**	K135-R142

[a] protein (p), rRNA (r), tRNA (t)

[b] Helix of 23S rRNA (H), helix of 16S rRNA (h), large subunit protein (L), small subunit protein (S).

[c] Amino acid residues and nucleotides are given in one letter code with residue number. *E. coli* ribosome numbering and domain assignment are based on ref.[4,5]. tRNA numbering is based on ref.[6].

Supplementary Table 2. Fractional populations, equilibrium constants, and transition rates for PRE^{-A}_{fMet} and PRE^{-A}_{Phe} complexes in the absence of EttA, in the presence of EttA, or in the presence of EttA-EQ_2.

			$smFRET_{L1\text{-}L9}$		
PRE^{-A}_{fMet}	% MS-I (%) [a]	% MS-II (%) [a]	K_{eq} [a]	$k_{MS\text{-}I \rightarrow MS\text{-}II}$ (sec^{-1}) [a]	$k_{MS\text{-}II \rightarrow MS\text{-}I}$ (sec^{-1}) [a]
– EttA	78 ± 2	22 ± 2	0.28 ± 0.03	0.44± 0.08	1.27 ± 0.12
EttA	88 ± 4	12 ± 4	0.14 ± 0.05	0.35 ± 0.13	2.07 ± 0.38
EttA-EQ_2	97 ± 1	3 ± 1	0.03 ± 0.01	N.D. [b]	N.D. [b]
			$smFRET_{L1\text{-}tRNA}$		
PRE^{-A}_{Phe}	% MS-I (%)	% MS-II (%)	K_{eq}	$k_{MS\text{-}I \rightarrow MS\text{-}II}$ (sec^{-1})	$k_{MS\text{-}II \rightarrow MS\text{-}I}$ (sec^{-1})
– EttA	72 ± 2	28 ± 2	0.39 ± 0.03	0.55 ± 0.10	0.78 ± 0.07
EttA	73 ± 2	27 ± 2	0.37 ± 0.05	0.52 ± 0.05	0.79 ± 0.29
EttA-EQ_2	96 ± 2	4 ± 2	0.04 ± 0.02	N.D. [b]	N.D. [b]

[a] Mean ± standard deviation (mean ± s.d.) of equilibrium constants, fractional population of MS-I and MS-II, and transition rates for each PRE^{-A} complex, were calculated as described in Supplementary Methods from three independent data sets.

[b] stands for not determined.

SUPPLEMENTARY NOTES

Limitations in interpreting some structures of ribosomes with bound translation factors

Interpretation of ribosome structures with some translation factors has been impeded by uncertainty as to their exact physiological and biochemical activities. For example, cryo-EM studies show that eukaryotic Elongation Factor 3 (eEF3), a fungal-specific essential translation factor belonging to a third different phylogenetic lineage in the ABC superfamily, binds over the E site of the ribosome at the interface between its small and large subunits[7]. However, eEF3 has been proposed, alternatively, to promote release of deacylated tRNAs from the E site[8] or to dissociate the small and large ribosomal subunits to recycle them from post-termination complexes[9]. Interpretation of the cryo-EM structure of ribosome-bound eEF3 has been complicated by the conflicting data on its biochemical function[8-10]. Another example is provided by the Ribosome Modulation Factor (RMF), which promotes storage of inactive ribosomes in stationary phase cells by driving the formation of a non-covalent dimer of 70S ribosomes[11,12]. An X-ray crystal structure has been determined for *E. coli* RMF bound to the mRNA exit channel of ribosomes from *T. thermophilus*[13], although RMF orthologs are not found in that organism or any organism outside the proteobacterial phylum. The crystal structure of the heterologous complex showed an allosteric conformational change in the small ribosomal subunit, which was interpreted as driving ribosome dimerization even though a ribosome dimer was not observed in that structure[13]. While *E. coli* RMF induces dimerization of *T. thermophilus* ribosomes in solution, the structural model proposed based on the crystal structure of the heterologous complex has not been tested[13]. A third example is provided by the widely conserved translation factor Elongation Factor P (EF-P)[14,15]. An X-ray crystal structure was determined for *T. thermophilus* EF-P bound between the E and P sites in a ribosome from the same organism[16]. This structure was interpreted based on earlier biochemical results supporting a role in promoting formation of the first peptide bond during the transition from the initiation to the elongation stage of protein translation[14]. However, more recent genetic[17] and biochemical[18] studies demonstrated that EF-P instead prevents ribosome stalling during translation of poly-proline (Pro) sequences (PPP or PPG). The structure has yet to be reinterpreted in light of these updated biochemical findings.

Parallels between the putative mechanisms of EttA and EF-P

There are several noteworthy parallels between the mechanism proposed here for EttA and that previously proposed for the essential elongation factor EF-P. While EF-P is much smaller than EttA (188 *vs.* 555 amino acids) and does not have any structural homology, it binds at a location partially overlapping with EttA's binding site, between the P and E sites on the 70S ribosome[16], and it also contacts the P-site tRNA on the ribosome (Fig. 3d). As described in the introduction, EF-P prevents elongating ribosomes from stalling on poly-Pro sequences, possibly by promoting peptide-bond formation in the PTC when a peptidyl-tRNA^{Pro} with two or more C-terminal Pro residues is bound in the P site on the ribosome[18]. Contrary to conclusions from much older studies, recent data have shown that EF-P does not have any specificity for formation of the first peptide bond in the nascent protein[19], which occurs concomitantly with the entry of the 70S IC into the translational elongation cycle. While Boel *et al.* show that EttA does have such specificity[1], it is noteworthy that initiator tRNA^{fMet}, which is bound in the P site of the ribosome

in 70S IC, and $tRNA^{Pro}$ share the CpU bulge, which is not found in any other *E. coli* tRNAs. Residues 65-68 in domain II of *T. thermophilus* EF-P are within hydrogen bonding distance of the CpU bulge in the P-site tRNA in the crystal structure of the corresponding ribosomal complex[16], while residues 434-436 in the ***α***-helical domain of ABC2 in EttA are proximal to this structural feature of the initiator $tRNA^{fMet}$ bound in the cryo-EM structure reported here (Fig. 5 and Supplementary Table 1). These observations suggest that recognition of the CpU bulge is a property shared by the only two translation factors known to bind in the ribosomal E site.

It is also worth noting that both EF-P and EttA have been proposed to modulate the conformation of the PTC to control the peptidyl-transferase activity of the ribosome when a tRNA containing the CpU bulge is bound in the P site on the ribosome. The authors of the recent work on EF-P speculate that it modulates the conformation of the substrate in the PTC to enhance catalysis of peptide bond formation when a peptidyl-$tRNA^{Pro}$ bound in the P site of the ribosome has multiple C-terminal Pro residues[18]. Similarly, as described above, the structural and biochemical studies of EttA reported here and in Boel *et al.*[1] suggest that, when initiator $tRNA^{fMet}$ is bound in the PTC, EttA has divergent allosteric effects on catalysis of peptide-bond formation in the presence of ADP *vs.* ATP. EttA substantially inhibits peptide-bond formation in the presence of ADP, while stimulates it slightly in the presence of ATP. Additional studies will be required to understand the biochemical and structural principles underlying the inferred activities of EF-P and EttA in modulating catalysis of peptide-bound formation in the PTC and determine whether the CpU bulge plays an important role in these activities.

Supplementary Methods

Pull-down of 70S ribosome with His_6-EttA-EQ_2. Strain MG1655-*ettA::Tn5* carrying either the plasmids, pBAD-*ettA*, pBAD-His_6-*ettA* or pBAD-His_6-*ettA*-EQ_2[1] were grown over-night in LB media (Affymetrix/USB) with ampicillin at 100 μg/ml and Glucose at 0.4% (to repress plasmid expression). The next morning, fresh LB ampicillin cultures (1 liter each) were inoculated with the over-night cultures, induced with L-arbinose (0.05 %) at OD_{600} of 0.5 and then grown for an extra 2 h. Cells were centrifuged at 4,000 rpm for 30 min (JS-4.2 rotor in Beckman J6-B) and washed with Phosphate Buffered Saline (137 mM NaCl, 2.7 mM KCl, 10 mM, Na_2HPO_4, 2 mM KH_2PO_4) and centrifuged for 10 min at 6,000 rpm (GSA rotor in Sorval RC5-B) then the pellets were stored at -80 °C. Pellets were resuspended (10 ml for pBAD-*ettA* and pBAD-His_6-*ettA,* 5 ml for pBAD-His_6-*ettA*-EQ_2 since this construct inhibits bacteria growth) in lysis buffer (25 mM Tris acetate pH 7.6, 2 mM $Mg(OAc)_2$, 60 mM KOAc, 10% Glycerol, 2 mM 2-mercaptoethanol, 2.5 mM ATP, EDTA free Complete Protease Inhibitor Cocktail Tablets (Roche) and 10 mM imidazole). Cells were incubated 10 min on ice with 2 mg/ml of lysozyme (Sigma-Aldrich) and lysed using 3 passages through an Emulsiflex C3 (Avestin) at 16,000 psi. Lysates were centrifuged at 30,000 g for 30 min and total protein concentration was estimated by Bradford test (Bio-Rad). An equal amount of total protein for each sample was loaded on three columns of 1 ml Ni-NTA (Qiagen), washed with 15 column-volumes of buffer A (same as lysis buffer but without protease inhibitor) then 15 column-volumes of buffer B (same as buffer A but with imidazole at 30 mM) and finally the protein was eluted and fractioned with buffer C (same as buffer A but with imidazole at 300 mM). The fractions of the sample pBAD-His_6-*ettA* and pBAD-His_6-*ettA*-EQ_2 were first run on a Mini-Protean (Bio-Rad) SDS-PAGE gel to determine

the amount of EttA. Then the fractions were diluted to have the same amount of EttA between the sample pBAD-His_6-*ettA* and pBAD-His_6-*ettA*-EQ_2 and loaded on a 20 × 20 cm, 4% to 20% SDS-PAGE gel (Bio-Rad). For the control, 60 µl of EttA without tag was loaded, which was the maximum volume of the well. The gel was stained with Coomassie blue and the bands of interest were excised from the gel for peptide mass fingerprinting identification.

Peptide mass fingerprinting identification. Bands were treated as described by Boël *et al.*[20] but the digestion was done with sequencing-grade trypsin (Promega) at 0.1 µg/ml. Resulting peptides were desalted using C18 ZipTip (Millipore) and eluted in 10 µl of 50% acetonitrile, 0.1% (v/v) trifluoroacetic acid. For each sample, 1 µl of the peptides was spot on the Voyager De Pro MALDI-TOF (Applied Biosystems) plate with 1 µl of ***α***-cyano-4-hydroxycinnamic acid in 50% acetonitrile , 0.1% trifluoroacetic acid. Peptides were detected using constructor setup for peptide detection with a-cyano-4-hydroxycinnamic as matrix. Calibration was done using MS Peptide Standards (NE Biolab). Data post-processing was done with the Data Explorer software (Applied Biosystems), protein identification by peptide profiling was done using the Aldente software[21] (previously on ExPASy, http://expasy.org/, now part of Genebio).

Purification by gel-filtration chromatography. 5 liters culture of the strain MG1655-*ettA::Tn5* carrying pBAD-His_6-*ettA*-EQ_2 was grown and the cells were processed as described above with lysis volume and column volume increased 5 fold. The fraction 1 to 5 after Ni-NTA pull-down were pooled, concentrated and run on a Sephacryl S300HR gel filtration column (GE Healthcare) equilibrated in buffer: 25 mM Tris acetate pH 7.6, 2 mM $Mg(OAc)_2$, 60 mM KOAc, 2 mM 2-mercaptoethanol and 0.5 mM Mg-ATP. The fractions of first peak corresponding to a size superior to 1.5 MDa (void volume) were pooled and concentrated in the same buffer on an Amicon Ultra 100 kDa (Millipore). The sample was separated on a 15% SDS-PAGE gel (Bio-Rad) and also submitted to western blotting using an anti-EttA antibody (methods described in[1]).

Cryo-EM data computational classification. The cryo-EM map of the total dataset revealed weaker densities for the A- and P-site tRNAs relative to 23S rRNA of the 50S subunit, indicating heterogeneity in the total dataset, i.e. ribosome particles being in different conformations and/or containing different components. Therefore we used the RELION[22,23] program in a stepwise hierarchical classification (**Supplementary Fig. 3**). The reference volume for initial alignment was the 3D reconstruction of the total dataset, refined using SPIDER and then low-pass filtered to 60 Å. An objective criterion to determine the optimal number of classes to start each classification step has yet to be established[22]. In practice, we choose the number of classes that is bigger than the expected number, in order to accommodate unexpected classes, and, after classification, consolidate classes yielding similar 3D reconstructions as judged by visual examination.

In step (1), the total dataset (108,691 particles) was separated into 10 classes using RELION[23] with 0.9º-step local angular search. Among these 10 classes, 3 classes yielded similar 3D reconstructions of 70S ribosome complexes containing EttA and P- and A-site tRNAs (denoted as 70S–EttA–$tRNA_2$ classes, red circle). Another 6 classes yielded 3D reconstructions of 70S ribosome complexes containing EttA, and either only P-site tRNA (denoted as 70S–EttA–tRNA class, magenta) or very weak densities for tRNAs (denoted as 70S–EttA class, blue). The other class (gray, 8.0% of total particles) was excluded from downstream analysis because the 3D

reconstruction indicated the presence of particles containing 50S large subunit only. In step (2), the three 70S–EttA–$tRNA_2$ classes were grouped and classified again; but no other conformations could be detected, confirming the homogeneity of this class. The 70S–EttA–tRNA and 70S–EttA classes were grouped together and classified, because these 3D reconstructions only show a local difference regarding P-site tRNA occupancy. The 3D reconstructions were sorted into new 70S–EttA–tRNA and 70S–EttA classes, based on the presence and intensity of P-site tRNA density. In step (3), the particles in 70S–EttA–tRNA and 70S–EttA classes from step (2), respectively, were grouped and classified again to ensure the homogeneity of each class. A small fraction of the particles were discarded from these two classes (5.7% and 3.6% of total particles, respectively), because they yielded poor-quality 3D reconstructions, in part due to limited number of particles per class.

The classification resulted in three final classes: the classes yielding 3D reconstruction of 70S ribosome complex containing EttA and strong densities of the P- and A-site tRNAs were grouped and designated as the final 70S–EttA–$tRNA_2$ class (class I, 39,316 particles, 36.2% of the total, 7.5 Å resolution). The classes yielding 3D reconstruction of 70S ribosome complex containing EttA and P-site tRNA were grouped and designated as the final 70S–EttA–tRNA class (class II, 16,639 particles, 15.3% of the total, 9.1 Å resolution). The classes yielding 3D reconstruction of 70S ribosome complex containing EttA only were grouped and designated as the final 70S–EttA class (class III, 33,889 particles, 31.2% of the total, 7.7 Å resolution). The 3D reconstructions of these three classes were separately refined by using RELION 3D auto-refine[23].

The class III may be mostly due to the saturating amount of 70S and EttA-EQ_2 ($fMet\text{-}tRNA^{fMet}$ 0.3 μM, 70S ribosome 0.45 μM, EttA-EQ_2 6 μM). Having similar resolutions (**Supplementary Fig. 4**), the 70S ribosomes in both cryo-EM maps of class I and class III are in the MS-I conformation. The 30S subunit in class III and that in class I exhibit the "30S domain closure" induced by cognate A-site tRNA binding, as observed by crystallography[24]. This 30S domain closure, together with the presence of A-site tRNA, differentiates class I from the other two classes. Moreover, the EttA density in class III and that in class I have similar global conformation, with 0.94 CCC between the two isolated density maps. Interestingly, one part of the PtIM density connecting to ABC2, attributable to EttA residues 303-306 in the MDFF-fitted structure, is poorly defined in the class III map but present in the class I map (**Supplementary Fig. 4b**, circled), suggesting that the PtIM is less structured in the absence of a P-site tRNA.

SUPPLEMENTARY REFERENCES

1. Boël, G. et al. The ABC-F protein EttA gates ribosome entry into the translation elongation cycle. *Nat. Struct. Mol. Biol.* (2013).
2. Finn, R.D. et al. The Pfam protein families database. *Nucleic Acids Res.* **38**, D211-D222 (2010).
3. Jühling, F. et al. tRNAdb 2009: compilation of tRNA sequences and tRNA genes. *Nucleic Acids Res.* **37**, D159-D162 (2009).
4. Yusupov, M.M. et al. Crystal structure of the ribosome at 5.5 Å resolution. *Science* **292**, 883-896 (2001).
5. Voorhees, R.M., Weixlbaumer, A., Loakes, D., Kelley, A.C. & Ramakrishnan, V. Insights into substrate stabilization from snapshots of the peptidyl transferase center of the intact 70S ribosome. *Nat. Struct. Mol. Biol.* **16**, 528-533 (2009).
6. Steinberg, S., Misch, A. & Sprinzl, M. Compilation of tRNA sequences and sequences of tRNA genes. *Nucleic Acids Res.* **21**, 3011-3015 (1993).
7. Andersen, C.B.F. et al. Structure of eEF3 and the mechanism of transfer RNA release from the E-site. *Nature* **443**, 663-668 (2006).
8. Triana-Alonso, F.J., Chakraburtty, K. & Nierhaus, K.H. The elongation factor 3 unique in higher fungi and essential for protein biosynthesis is an E site factor. *J. Biol. Chem.* **270**, 20473-8 (1995).
9. Kurata, S. et al. Ribosome recycling step in yeast cytoplasmic protein synthesis is catalyzed by eEF3 and ATP. *Proc. Natl. Acad. Sci. U. S. A.* **107**, 10854-10859 (2010).
10. Kamath, A. & Chakraburtty, K. Role of yeast elongation factor 3 in the elongation cycle. *J. Biol. Chem.* **264**, 15423-8 (1989).
11. Yoshida, H. et al. The Ribosome Modulation Factor (RMF) binding site on the 100S ribosome of *Escherichia coli*. *J. Biochem. (Tokyo).* **132**, 983-989 (2002).
12. Yoshida, H., Yamamoto, H., Uchiumi, T. & Wada, A. RMF inactivates ribosomes by covering the peptidyl transferase centre and entrance of peptide exit tunnel. *Genes Cells* **9**, 271-278 (2004).
13. Polikanov, Y.S., Blaha, G.M. & Steitz, T.A. How hibernation factors RMF, HPF, and YfiA turn off protein synthesis. *Science* **336**, 915-918 (2012).
14. Glick, B.R. & Ganoza, M.C. Identification of a soluble protein that stimulates peptide bond synthesis. *Proc. Natl. Acad. Sci. U. S. A.* **72**, 4257-60 (1975).
15. Aoki, H., Adams, S.L., Turner, M.A. & Ganoza, M.C. Molecular characterization of the prokaryotic *efp* gene product involved in a peptidyltransferase reaction. *Biochimie* **79**, 7-11 (1997).
16. Blaha, G., Stanley, R.E. & Steitz, T.A. Formation of the first peptide bond: the structure of EF-P bound to the 70S ribosome. *Science* **325**, 966-970 (2009).
17. Ude, S. et al. Translation elongation factor EF-P alleviates ribosome stalling at polyproline stretches. *Science* **339**, 82-85 (2013).
18. Doerfel, L.K. et al. EF-P is essential for rapid synthesis of proteins containing consecutive proline residues. *Science* **339**, 85-88 (2013).
19. Bullwinkle, T.J. et al. (R)-beta-lysine-modified elongation factor P functions in translation elongation. *J. Biol. Chem.* **288**, 4416-23 (2013).

20. Boël, G. et al. Is 2-phosphoglycerate-dependent automodification of bacterial enolases implicated in their export? *J. Mol. Biol.* **337**, 485-496 (2004).
21. Palagi, P.M. Two-dimensional electrophoresis protocols database interrogation algorithms for identification of proteins in proteomic separations. *Methods Mol. Biol.* **519**, 515-531 (2009).
22. Scheres, S.H.W. A Bayesian view on cryo-EM structure determination. *J. Mol. Biol.* **415**, 406-418 (2012).
23. Scheres, S.H.W. RELION: Implementation of a Bayesian approach to cryo-EM structure determination. *J. Struct. Biol.* **180**, 519-530 (2012).
24. Ogle, J.M., Murphy Iv, F.V., Tarry, M.J. & Ramakrishnan, V. Selection of tRNA by the ribosome requires a transition from an open to a closed form. *Cell* **111**, 721-732 (2002).